# Polycyclic aromatic hydrocarbons removal from aqueous solution with PABA-MCM-41/polyethersulfone mixed matrix membranes

**José Arnaldo S. Costa** (✉ josearnaldo23@yahoo.com.br)
Universidade Federal de Sao Carlos Centro de Ciencias Exatas e de Tecnologia https://orcid.org/0000-0002-2354-1163

**Victor H. V. Sarmento**
Federal University of Sergipe: Universidade Federal de Sergipe

**Luciane P. C. Romão**
Federal University of Sergipe: Universidade Federal de Sergipe

**Caio M. Paranhos**
Federal University of Sao Carlos: Universidade Federal de Sao Carlos

**Research Article**

**Keywords:** Mesoporous array, mixed matrix membrane, environmental remediation, transport properties, PAHs.

**Posted Date:** March 24th, 2021

**DOI:** https://doi.org/10.21203/rs.3.rs-339127/v1

# Abstract

Polycyclic aromatic hydrocarbons (PAHs) are one of the most recalcitrant pollutant originated from the burning of coal, petroleum, and other fossil fuels. The human exposure to PAHs may contribute to develop several carcinogenesis mechanisms. The aim of the present study was to develop a mixed matrix membrane (MMM) based on polyethersulfone (PES) and functionalized mesoporous material for the remediation of PAHs mixture by adsorption processes. MCM-41-based mesoparticles were obtained from biomass reuse of rice husk ash (RHA) and functionalized with *p*-aminobenzoic acid (PABA). The hydrothermal and casting methods were effective and sustainable in the preparation of PABA-MCM-41 and PES-based MMMs, respectively. PES-based MMMs presented an excellent distribution of the arrays incorporated and small-angle ordering. The absorption of PAHs was influenced by the incorporation of PABA-MCM-41 within the PES matrix.


# 1. Introduction

Polymeric membranes have been increasingly required in separation processes of different pollutants [1]. The systematic use of polymer membranes is mainly due to their main characteristics such as: energy efficiency, easy preparation, selectivity, low-cost, high mechanical resistance, eco-friendly, and recyclability [2–4]. In this way, membrane technology has been applied in the most different research front, such as gas separation [2, 5–7], $CO_2$ [8, 9], heavy crude oil [10], metal [11–13], and organic compounds removal [14–17], catalysis [18, 19], fuel cell [20–23], distillation processes [24–26], drug release [27–29], among other applications.

Recently, alternatives have been sought to improve the performance of conventional polymer membranes, this from the incorporation of nanoparticles into the polymer matrix. Thus, this new trend is called mixed matrix membranes (MMMs), which combine the properties of polymer matrix with the filler material. [6, 30]. Thus, the performance of MMMs can be influenced by different factors, mainly: **(i)** characteristics of polymer and architecture of the filler material, **(ii)** compatibility, and **(iii)** preparation technique of MMMs [31].

Multifunctional mesoporous arrays have interesting properties to be used as fillers material in MMMs. The M41S-based mesoporous matrixes are known to have elevated surface area, thermal and mechanical stability, uniform mesoporous distribution, and high pore volume values, which can enable the flow of small molecules. In addition, mesoporous materials can be easily functionalized, as well as presents high adsorption capacity [32–38].

In this sense, membranes can play a crucial role in the separation process of emerging contaminants. Among the main organic pollutants that are released in the environment are polycyclic aromatic hydrocarbons (PAHs) [32, 36, 38]. PAHs are mainly from the exploration of petroleum, combustion of fossil fuels, and automobile exhaust emissions, which are classified as non-biodegradable, mutagenic, allergenic, teratogenic, toxic, and/or carcinogenic compounds by the International Agencies [39, 40].

In this investigation, modified mesoporous structure prepared from RHA was applied as filler array in polyethersulfone (PES) MMMs to be tested in the PAHs remediation from aqueous media. The MCM-41-based mesoparticles obtained from biomass were modified with PABA group. Our research group has demonstrated that PABA-MCM-41 is a potential good absorbent for PAHs [32, 41]. From our knowledge, there are few investigations on the use of functionalized mesoporous materials in MMMs for PAHs remediation from aqueous media. Consequently, the present work can contribute significantly to the evaluation of a low-cost and eco-friendly biomass-based membrane for field of wastewater treatment.

# 2. Experimental

## 2.1. Materials

The RH was provided from the Embrapa, São Carlos, Brazil. The RHA obtained from the thermal treatment carried out on the RH and the characterizations of both were previously reported [42]. The B[b]F, B[k]F, and B[a]P analytical standards (> 96.0% purity) were purchased from Aldrich. The solvent utilized was HPLC-grade acetonitrile (99.9%, Tedia). Ammonia monohydrate ($NH_3.H_2O$, Synth), 3-(triethoxysilyl)propyl isocyanate (TEPIC, Aldrich), Cetyltrimethylammonium bromide (CTAB, 98.0%, NEON), p-aminobenzoic acid (PABA, ≥99.0%, Aldrich), polyethersulfone (PES, RADEL), chloroform ($CHCl_3$, Synth), and phosphorus pentoxide ($P_2O_5$, Aldrich) were all utilized with no further purification, and the ultrapure water was obtained from a Milli-Q system (Millipore Co.).

## 2.2. Synthesis of the PABA-MCM-41 (RHA) functionalized mesoporous material

The synthesis of functionalized mesoporous material was performed previously by our group from the hydrothermal/co-condensation method [43].

## 2.3. Preparation of MMMs

The membranes were made according to the methodology reported by Khan et al. [44], with modifications: PES and PABA-MCM-41 mesoporous material were dried at 85 and 150 ºC for 2 h, respectively. A solution of 20 wt.% PES was prepared in chloroform under constant stirring for 24 h. The resulting solution was casts on a petri dish and covered by an inverted glass funnel. At the end of 24 h, the funnel was removed to evaporate the residual solvent under ambient conditions (24 h). The pure PES membrane was then dried for 12 h (85 ºC) in a vacuum oven to further remove the residual solvent.

The preparation of the PES/PABA-MCM-41 MMMs adopted the following procedure: amounts of the PABA-MCM-41 in range 1-10.0 wt.% were dispersed under magnetic stirring in the PES solution for 24 h at room temperature. Finally, the same procedure to obtaining the pristine PES membrane was performed.

## 2.4. Transport properties of MMMs

### 2.4.1. Water vapor transport (WVT)

WVT experiments were realized according to ASTM E96 [45] and as previously shown in [14].

### 2.5.1. Water static sorption

The assays were realized in ultrapure water, in which the PES-based MMMs were weighed and submerged in water until to 15 days, after which they were weighed again, and the swelling percentage was assessed from the expression:

$$\% \text{ Swelling} = \left(\frac{m_f - m_i}{m_i}\right) \times 100, \quad (3)$$

where $m_i$ and $m_f$ are the initial and final masses (g), respectively.

### 2.5.2. Permeation/absorption of the PAHs

The permeation assessment was performed at room temperature using a side-by-side glass diffusion cell with two independent compartments separated by the PES-based MMMs. The PES-based MMMs were introduced between the two compartments of the cell and the system was sealed (constant pressure of 1.1 MPa, and membrane contact area between the glass cells of ~2.31 $cm^2$). All permeation assays were performed using a volume of 35 mL on each side of the cell under magnetic stirring, and the feed phase was filled with a solution containing the PAHs mixture (B[b]F, B[k]F, and B[a]P). These assays were conducted using an initial PAHs concentration of 200 μg $L^{-1}$, solution pH 5.6, and magnetic stirring at 150 rpm. PAHs concentrations were obtained by sampling of 0.5 mL of each compartment at certain time intervals in the range of 0-48 h and B[b]F, B[k]F, and B[a]P quantities were measured in an HPLC equipment attached with a fluorescence detector (Shimadzu, Japan). The results found were shown in terms of the permeation rate (*PR*), calculated using the expression:

$$PR = \frac{C_{P,48h}}{C_{F,0h}} \times 100, \quad (4)$$

where *PR* is the permeation rate (%), $C_{F,0h}$ is the initial concentration of PAHs of feed phase (μg $L^{-1}$) and $C_{P,48h}$ is the PAHs concentration of permeate phase after 48 h (μg $L^{-1}$).

### 2.6. Determination of B[b]F, B[k]F, and B[a]P PAHs

Polycyclic aromatic hydrocarbons were quantified on an HPLC using a Shimadzu LC-20A Prominence equipment according to the methodology developed in our research group [46], and the $r^2$ values obtained were 0.997, 0.999, and 0.999 for B[a]P, B[b]F, and B[k]F, respectively.

### 2.7. Characterizations

The ATR-FTIR spectra of PES-based MMMs were measurement in a Varian 3100 spectrophotometer (at room temperature, 4000-600 $cm^{-1}$ region, resolution of 2 $cm^{-1}$, and 20 scans). The materials were analyzed by XRD in a Shimadzu LabX XRD-6000 diffractometer operating with Cu Kα (λ = 1.5406 Å, room temperature, $2\theta$ range of 5-50º, width of 0.02º, step time of 0.6 s, and a scanning rate of 2º $min^{-1}$. SAXS assays were done according to the previously reported methodology [32]. SEM was required in a Phillips FEGXL 30/EDS equipment (3 kV). DSC analyzes of the PES-based MMMs were realized in a NETZSCH DSC 200 *F3* apparatus (50 mL $min^{-1}$ flow of nitrogen). Heating and cooling cycles between 20-240 ºC (20 ºC $min^{-1}$) and the glass transition temperature (Tg) of PES-based MMM was determined in the second heating by the inflection point method.

# 3. Results And Discussion

## 3.1. Characterizations

The characterizations of the RH and RHA materials are reported previously [42, 47]. The PABA-MCM-41 (RHA) modified mesoporous array exhibited a hexagonal arrangement with surface area value of the magnitude of 438 $m^2$ $g^{-1}$, the $N_2$ adsorption/desorption analysis also revealed a type IV isotherm with H1 hysteresis. Finally, the mesoporous structure showed an excellent thermal stability and total pore volume and pore diameter values of 0.41 $cm^3$ $g^{-1}$ and 3.59 nm, respectively [43]. In addition, the PABA-MCM-41 (RHA) presented the same typical bands of the modified mesoporous array, as demonstrated previously [36].

Figure 1(i) shows the ATR-FTIR spectra obtained for the pristine PES membrane and the MMMs prepared with the PABA-MCM-41 (RHA) in percentages between 1.0–10.0 wt.%. It is possible to observe the main characteristic bands of the PES, which are centered in the range between 2962 – 2839 $cm^{-1}$ and those at around 831, 799, and 689 $cm^{-1}$ are assigned to the stretching and vibration of C–H bond of the backbone of the aromatic hydrocarbon of PES, respectively [48, 49]. The band centered at 1408 $cm^{-1}$ is assigned to the – $CH_3$ bond of the $CH_3$ – C–$CH_3$ group [49, 50]. The band at 1231 $cm^{-1}$ and those between 872 – 856 $cm^{-1}$ are attributed to the asymmetric vibration of the ether group [48, 50].

The bands around 1321, 1296 and 1009 $cm^{-1}$ can be assigned to the symmetrical and asymmetric O = S = O vibrations of the sulfone group, as well as the bands near 1145 and 1100 $cm^{-1}$ are attributed to the S = O elongation. The bands around 1577 and 1483 $cm^{-1}$ belonging to the C = C bond of the aromatic groups of PES [48, 51, 52].

The spectra of PES-based MMMs show an increase of the band intensity between 2962 – 2839 $cm^{-1}$. These bands are attributed to the vibrations of the methylene groups (–(– $CH_2)_3$–) of the PABA-Si present into the PABA-MCM-41 functionalized mesoporous material [36, 43], as well as the appearance of a band at around 1725 $cm^{-1}$ on the MMMs, which can be assigned to the C = O stretching of carboxylic acid present on the PABA-Si functional group from PABA-MCM-41 (RHA). Likewise, the new band close to

1535 $cm^{-1}$ is assigned to the amide – CONH – vibrations of PABA-Si groups [36], confirming that there was a good dispersion of mesoparticles on the PES MMMs.

The presence of the main bands of PES on the MMMs confirms the compatibility between the mesoparticles and the polymer chains. In this way, a decrease in the intensity of the bands close to 1321, 1296, and 1009 $cm^{-1}$ (O = S = O symmetric and asymmetric vibrations), 1145 and 1100 $cm^{-1}$ (elongation of S = O bond), and the bands centered at around 1577 and 1483 $cm^{-1}$ (C = C bond of aromatic groups of PES) with the increase of the PABA-MCM-41 amount. Therefore, this decrease is attributable to the interaction between these PES groups with the carboxylic acid groups (– $CO_2H$) present within the PABAMCM-41 arrays. However, the characteristic bands of amorphous silica of the PABA-MCM-41 were not evidenced in the spectra of the MMMs because of the overlapping of these bands in the presence of PES.

Figure 1(ii) shows the X-ray diffractograms obtained of PABA-MCM-41 (RHA), pristine PES membrane, and MMMs. The PABA-MCM-41 and the PES membrane exhibited a single diffraction peak, which is attributed to the amorphous halo of the silica source used on the PABA-MCM-41 and the amorphous structure of PES, respectively. It is also possible to observe that the MMMs presented the same wide band observed for the pristine membrane. This behavior is due to the compatibility between PABA-MCM-41 mesoparticles and the PES matrix.

Figure 1(iii) shows the SAXS profiles obtained of pristine membrane and MMMs. The PABA-MCM-41 array exhibited a ratio of relative distances of 1:√3:2, derived from the peaks ratio ($q_{100}/q_{100}$, $q_{110}/q_{100}$, and $q_{200}/q_{100}$), respectively, confirming the mesoporous pattern of PABA-MCM-41 [43]. However, the pristine membrane did not present SAXS profile. Conversely, the PES-based MMMs presented three peaks at around the scattering vector $q_{100}$, $q_{110}$, and $q_{200}$ related to the (100), (110), and (200) planes from the PABA-MCM-41 within the MMMs. Furthermore, there was an increase in peak intensity $q_{100}$ with increase in the proportion of mesoparticles within the MMMs.

Figure 1(iv) shows the DSC curves of the second heating obtained of the pristine membrane and MMMs, while Table 1 shows the glass transition temperature (Tg) values found for same samples. There was only one thermal event for all samples, which is associated with the glass transition, where it is possible to observe a small decrease in Tg values of the PES-based MMMs compared to pristine membrane. The presence of the mesoparticles within the PES matrix seems to facilitate the flexibility of PES chain of PES-based MMMs in the interface PES/PABA-MCM-41.

Table 1
Glass transition temperature (Tg) values of pristine PES membrane and PES-based MMMs.

| Polymer membrane | | $T_g$ |
|---|---|---|
| **Polymer** | **PABA-MCM-41 (RHA)** (wt.%) | (°C) |
| **PES** | **0.0** | 223.4 |
| | **1.0** | 221.1 |
| | **2.5** | 221.6 |
| | **5.0** | 220.9 |
| | **7.5** | 222.2 |
| | **10.0** | 221.7 |

Figure 2 shows the SEM images obtained of the pristine membrane and PES-based MMMs. The pristine membrane (Fig. 2a) exhibits an asymmetrical structure with a dense layer at top and a sublayer in the form of elongated channels. In contrast, the MMMs show the appearance of interfacial voids surrounded by cavities at around mesoparticles incorporated.

The findings of the chemical compositions of the pristine membrane and PES-based MMMs obtained from the SEM-EDS analyzes are shown in Table 2. The C contents did not have significant changes for the MMMs compared to pristine membrane, the same behavior was seen for the impurity contents of Cr, Al, Fe, and Ca. On the other side, the Si and O contents increased with the increase in the percentage of PABA-MCM-41, but the same was not noticed for S and Cl contents.

Table 2
Chemical composition of pristine PES membrane and PES-based MMMs determined by SEM-EDS.

| **Polymer membrane** | | **Analyte (%)** | | | | | | | | |
|---|---|---|---|---|---|---|---|---|---|---|
| **Polymer** | **PABA-MCM-41 (RHA)** (wt.%) | **C** | **O** | **Si** | **S** | **Cl** | **Cr** | **Al** | **Fe** | **Ca** |
| | **0.0** | 61.07 | 10.30 | 0.15 | 18.92 | 9.11 | 0.02 | 0.01 | 0.35 | 0.12 |
| | **1,0** | 59.28 | 20.57 | 1.14 | 13.59 | 3.34 | 0.11 | 0.01 | 1.03 | 0.99 |
| | **2,5** | 55.93 | 23.30 | 3.47 | 13.74 | 3.09 | 0.04 | 0.02 | 0.26 | 0.16 |
| **PES** | **5,0** | 53.11 | 20.25 | 5.77 | 11.77 | 7.29 | 0.00 | 0.12 | 0.76 | 0.92 |
| | **7,5** | 59.47 | 16.24 | 8.62 | 8.22 | 5.68 | 0.00 | 0.14 | 1.41 | 0.23 |
| | **10,0** | 51.97 | 20.67 | 8.52 | 12.38 | 5.55 | 0.00 | 0.10 | 0.20 | 0.65 |

### 3.2. Absorption of MMMs

The WVT and *P* values for the pristine PES and MMMs are shown in Table 3. The WVT values for the MMMs were higher than the value obtained for the pristine membrane. The same behavior was also observed for the *P* values, except in MMM with 1.0 wt.% of mesoparticles. This phenomenon occurs due to the increase in the number of preferred paths for the water vapor transport with the incorporation of the mesoporous material within the MMMs, as seen in the SEM results.

Table 3
Water vapor transport (WVT) and permeation (*P*) values obtained for pristine PES membrane and PES-based MMMs

| **Polymer membrane** | | **WVT** | ***P*** |
|---|---|---|---|
| **Polymer** | **PABA-MCM-41 (RHA) (wt.%)** | **(g $h^{-1}$ $m^{-2}$)** | ***x*** **$10^{-11}$ (g $Pa^{-1}$ $s^{-1}$ $m^{-1}$)** |
| | 0.0 | 1.68 | 2.03 |
| | 1.0 | 3.25 | 1.93 |
| | 2.5 | 2.27 | 2.17 |
| **PES** | 5.0 | 2.27 | 2.45 |
| | 7.5 | 2.04 | 2.22 |
| | 10.0 | 2.83 | 2.70 |

Figure 3(a) shows the correlation between the *P* and Tg values of the MMMs. It is possible to observe an inverse relationship between *P* and Tg values, except for MMM with 1.0 wt.%. This behavior occurs because at low Tg values, there is a greater mobility of the polymer chains, thus facilitating the permeation process through these MMMs.

Table 4 presents the water static sorption values for the pure PES membrane and MMMs. There was a decrease in the swelling degree after incorporation of 1.0 wt.% of PABA-MCM-41 in the PES matrix. This behavior can be related to the occupation of the PES free volume by the well dispersed mesoparticles. However, for the 2.5, 7.5, and 10.0 wt.% contents, the swelling degree values were higher than those obtained for the other MMMs, and this can also be related to the occupation of the water molecules in the pores of the mesoparticles within the MMMs.

Table 4
Water static sorption values obtained for pristine PES membrane and PES-based MMMs.

| **Polymer membrane** | | **Swelling degree (%)** |
|---|---|---|
| **Polymer** | **PABA-MCM-41 (RHA) (wt.%)** | |
| | 0.0 | 1.78 |
| | 1.0 | 0.49 |
| | 2.5 | 7.69 |
| **PES** | 5.0 | 1.60 |
| | 7.5 | 3.46 |
| | 10.0 | 2.51 |

Figure 3(b) shows the correlation of the swelling degree with the Tg values for the MMMs. There is a direct correlation between the mentioned values, so an increase in Tg causes an increase in the amount of water imprisoned in the free volume of the polymer matrix, as well as in the pores of PABA-MCM-41. In contrast, this behavior reflected in lower *P* values (Fig. (3a)), because of the strong imprisonment of the water molecules by the silanol and PABA-Si groups of the modified mesomaterial structure within the PES-based MMMs.

Figure 4(a-c) shows the results found from the PAHs concentration in feed solution against time for PES-based MMMs. The increase in the operation time caused a decrease in the PAHs concentrations since the equilibrium time found was at around 24 h for all MMMs. As with the final PAHs concentrations of the pristine membrane, whose values were lower than those obtained for the PES-based MMMs.

In contrast, Fig. 4(d-f) shows the PAHs concentration values of permeated solution through the MMMs. An increase in the permeate concentration was observed as the operating time was longer, given that the equilibrium time found was in the order of 24 h. The values of the final concentrations permeated through the pristine membrane, for all PAHs, were lower than those obtained for the PES-based MMMs. However, these values are close to those found for the MMM with a content of 7.5 wt.% mesoparticles. In view of these results, we can suggest that the occupation of the free volume of PES by the mesoparticles facilitated the permeation of PAHs through these MMMs, due to the appearance of interfacial voids within the MMMs, as observed in the SEM analyzes.

Figure 4(g-i) shows the results of adsorbed concentrations of PAHs mixture by the pure PES membrane and MMMs. It is possible to note for all PAHs, that the pure PES membrane presented values of maximum concentration higher than those found for MMMs. On the other hand, the MMMs also presented relevant adsorption values. Therefore, the equilibrium time was reached in approximately 24 h for all MMMs. In summary, the preparation of MMMs with PABA-MCM-41 as filler material caused little interference in the transport property of PAHs. Since there was a slight increase in permeation of PAHs from the occupation of the free volume of PES polymer chains by the incorporated mesoparticles, as well as a decrease in adsorption of PAHs.

The results of permeation (*PR*) and retention (*RR*) rates and the removal percentage of PAHs mixture by PES-based MMMs were compiled in Table 5. The *PR* values observed for the PAHs mixture followed the following increasing order: B[b]F < B[k]F < B[a]P, due to the hydrophobic effect of PAHs mixture in solution. Therefore, for all PAHs, the respective *PR* values for the pristine membrane were lower than the values obtained for the MMMs, suggesting that the incorporation of PABA-MCM-41 into the PES facilitated the permeation of PAHs through the PES MMMs. However, the achieved values for the PES MMM with 7.5 wt.% were not so much higher than those found for the pristine membrane, as well as for the other MMMs.

Table 5
Permeation and retention rates and removal percentage values of PAHs mixture for PES-based MMMs.

| Polymer membrane | | PAH | Rate permeation (%) | Rate retention (%) | Removal percentage (%) |
|---|---|---|---|---|---|
| **Polymer** | **PABA-MCM-41 (RHA)** (wt.%) | | | | |
| **PES** | **0.0** | B[b]F | 1.670 | 98.330 | 83.004 |
| | | B[k]F | 4.666 | 95.334 | 79.676 |
| | | B[a]P | 5.574 | 94.426 | 79.190 |
| **PES** | **1.0%** | B[b]F | 2.190 | 97.810 | 44.628 |
| | | B[k]F | 5.028 | 94.972 | 47.095 |
| | | B[a]P | 6.016 | 93.984 | 51.103 |
| **PES** | **2.5%** | B[b]F | 2.121 | 97.879 | 53.781 |
| | | B[k]F | 4.893 | 95.107 | 55.317 |
| | | B[a]P | 5.949 | 94.051 | 59.680 |
| **PES** | **5.0%** | B[b]F | 2.544 | 97.456 | 61.746 |
| | | B[k]F | 4.939 | 95.061 | 55.833 |
| | | B[a]P | 6.162 | 93.838 | 60.160 |
| **PES** | **7.5%** | B[b]F | 1.783 | 98.217 | 44.604 |
| | | B[k]F | 4.668 | 95.332 | 48.597 |
| | | B[a]P | 5.606 | 94.394 | 65.988 |
| **PES** | **10.0%** | B[b]F | 2.364 | 97.636 | 43.333 |
| | | B[k]F | 5.023 | 94.977 | 46.050 |
| | | B[a]P | 6.322 | 93.678 | 40.696 |

In the *RR* values, which have an inverse relationship to the *PR* values, it was noted that the results found for the pristine PES membrane were higher than the results of the MMMs, except for MMM with 7.5 wt.%, whose *RR* values are close to the pristine membrane. On the other hand, the incorporation of PABA-MCM-41 within the MMMs caused a reduction of the removal percentage.

Figure 5(a-c) shows the correlation between the *PR* and $T_g$ values of PES-based MMMs. It is possible to observe an inverse relation between these values, except for MMM with 2.5 wt.%, in which the increase of

*PR* values occurred because of the decrease in $T_g$ values. This comportment can be attributed to the increase in the mobility of the PES chains, promoting more easily the permeation process of PAHs. However, this phenomenon was less meaningful for the MMM with 7.5 wt.% of mesoparticles.

On the contrary (Fig. (5d-f)), a direct relationship between the *PR* and *WVT* values. On the one hand, the decrease in Tg affected in the growth in the *PR* values. This decrease also boosted an increase in the *WVT* values. This comportment can be attributed to the growth in the number of preferred paths in the PES-based MMMs with the filling of mesoparticles, in addition to the mobility of the PES chains.

Similarly, to *PR* values, the *RR* values were also influenced by the $T_g$ values, as shown in Fig. 5(g-i). A direct relationship was observed between the *RR* and $T_g$ values, less for the MMM with 2.5 wt.%. In this way the decrease of the *RR* occurred due to the decay of Tg values. However, the decrease in $T_g$ was less evident for MMM with 7.5 wt.% of PABA-MCM-41. As a direct consequence, the decrease in retention rate (*RR*) was directly influenced by the increase of the permeation rate (*PR*) of PAHs mixture. In this way (Fig. 6(a-c)), it is possible to observe an inverse correlation between the *RR* and *WVT* values for PES MMMs.

Figure 6(d-f) and 6(g-i) present the correlations of the removal percentage of PAHs mixture with the Tg and WVT values, respectively. From Fig. 6(d-f), for some cases, that the removal percentage values do not have a defined relationship with the $T_g$ values. It was expected larger removal percentages at higher Tg values, as well as lower removal percentage values at lower Tg values. This behavior is due, respectively, to a greater or lesser ease of permeation of PAHs through the polymer chains of the MMMs. In this sense, this tendency was noted in the B[b]F and B[k]F removal, in the MMMs with 1.0 and 10.0 wt.%, as well as in the B[a]P removal in the contents of 1.0, 7.5, and 10.0 wt.% MMMs. These results show, for these MMMs, that the polymer matrix has more contribution in the adsorption of PAHs than the mesoporous array. But, for the other PES-based MMMs, we can observe an inverse relation between the removal percentage and Tg values, suggesting that the mesoporous array has a greater contribution in the adsorption of these PAHs than the PES matrix. Finally, from the analysis of Fig. 6(g-i), the removal percentage values of PAHs correlate inversely with the WVT values, except for the adsorption of B[b]F and B[k]F by the MMM with 7.5 wt.% MMMs.

# 4. Conclusion

In summary, we report the preparation of a novel mixed matrix membrane prepared with PES polymer and PABA-MCM-41 modified mesoporous array, which was applied in the PAHs removal. The hydrothermal/co-condensation method was useful, low-cost, and sustainable in the preparation of eco-friendly PABAMCM-41 matrix with an architectured hexagonal arrangement and interesting mesoparticles features. In the same way as the casting approach was useful in the formulation of the PES-based mixed matrix membranes, which exhibited a remarkable and efficient dispersion of the filled mesoparticles, noticed from its homogeneity seen in the SEM and SAXS results. So, the incorporation of mesoparticles into the polymer matrix altered the structural arrangement of PES-based MMMs, as well as caused a

small decrease in Tg values of MMMs when compared to the pristine PES membrane. The presence of the mesoparticles on the MMMs facilitated the mobility of polymer chain in the interface PES/PABA-MCM-41. Thus, in view of the permeation findings from PES-based MMMs, we can highlight that the transport features were guided by the filling of PABA-MCM-41 within the PES-based matrix.

# Declarations

### Compliance with ethical standards

### Consent for publication

The Authors transfer to Springer the publication rights.

### Availability of data and materials

The authors declare that data supporting the findings of this study are available within the article.

### Competing interests

The authors declare that they have no known competing financial interests or personal relationships that could have appeared to influence the work reported in this paper.


### Funding

The authors wish to thank Fundação de Amparo à Pesquisa do Estado de São Paulo (FAPESP) and Centro de Desenvolvimento de Materiais Funcionais for providing the essential financial support.


### Authors' contributions

**José Arnaldo S. Costa**: Conceptualization, Methodology, Validation, Investigation, Writing - Original Draft. **Victor H. V. Sarmento**: Conceptualization, Methodology, Investigation, Resources. **Luciane P. C. Romão**: Conceptualization, Methodology, Validation, Investigation. **Caio M. Paranhos**: Conceptualization, Methodology, Validation, Investigation, Resources, Writing - Review & Editing, Supervision, Project administration.


### Acknowledgments

The authors thank Fundação de Amparo à Pesquisa do Estado de São Paulo (FAPESP, Grants 2014/05679-4 and 2017/06775-5) and Centro de Desenvolvimento de Materiais Funcionais (CDMF, Grant 2013/07296-2) for the financial support.


# References

1. Dai Y, Niu J, Yin L, et al (2013) Laccase-carrying electrospun fibrous membrane for the removal of polycyclic aromatic hydrocarbons from contaminated water. Sep Purif Technol 104:1–8. https://doi.org/10.1016/j.seppur.2012.11.013
2. Bertelle S, Gupta T, Roizard D, et al (2006) Study of polymer-carbon mixed matrix membranes for CO2 separation from flue gas. Desalination 199:401–402. https://doi.org/10.1016/j.desal.2006.03.207
3. Scholes C, Scholes CA, Kentish SE, Stevens GW (2008) Carbon dioxide separation through polymeric membrane systems for flue gas applications Flue Gas Applications. 51–66. https://doi.org/10.2174/1874478810801010052
4. Brunetti A, Scura F, Barbieri G, Drioli E (2010) Membrane technologies for CO2 separation. J Memb Sci 359:115–125. https://doi.org/10.1016/j.memsci.2009.11.040
5. Arjmandi M, Pakizeh M (2014) Mixed matrix membranes incorporated with cubic-MOF-5 for improved polyetherimide gas separation membranes: Theory and experiment. J Ind Eng Chem 20:3857–3868. https://doi.org/10.1016/j.jiec.2013.12.091
6. Kim S, Pechar TW, Marand E (2006) Poly(imide siloxane) and carbon nanotube mixed matrix membranes for gas separation. Desalination 192:330–339. https://doi.org/10.1016/j.desal.2005.03.098
7. Basu S, Cano-Odena A, Vankelecom IFJ (2011) MOF-containing mixed-matrix membranes for CO2/CH4 and CO2/N2 binary gas mixture separations. Sep Purif Technol 81:31–40. https://doi.org/10.1016/j.seppur.2011.06.037
8. Mohshim DF, Mukhtar H, Man Z (2017) A study on carbon dioxide removal by blending the ionic liquid in membrane synthesis. Sep Purif Technol. https://doi.org/10.1016/j.seppur.2017.06.034
9. Neyertz S, Brown D (2016) Nanosecond-time-scale reversibility of dilation induced by carbon dioxide sorption in glassy polymer membranes. J Memb Sci 520:385–399. https://doi.org/10.1016/j.memsci.2016.08.003
10. da Costa Cunha G, Pinho NC, Alves Silva IA, et al (2019) Removal of heavy crude oil from water surfaces using a magnetic inorganic-organic hybrid powder and membrane system. J Environ Manage 247:9–18. https://doi.org/10.1016/j.jenvman.2019.06.050
11. Bao Y, Yan X, Du W, et al (2015) Application of amine-functionalized MCM-41 modified ultrafiltration membrane to remove chromium (VI) and copper (II). Chem Eng J 281:460–467. https://doi.org/10.1016/j.cej.2015.06.094
12. Bernardo P, Bazzarelli F, Tasselli F, et al (2017) Effect of physical aging on the gas transport and sorption in PIM-1 membranes. Polymer (Guildf) 113:283–294. https://doi.org/10.1016/j.polymer.2016.10.040
13. Gao A, Xie K, Song X, et al (2017) Removal of the heavy metal ions from aqueous solution using modified natural biomaterial membrane based on silk fibroin. Ecol Eng 99:343–348. https://doi.org/10.1016/j.ecoleng.2016.11.008

14. Costa JAS, Sarmento VHV, Romão LPC, Paranhos CM (2020) Removal of polycyclic aromatic hydrocarbons from aqueous media with polysulfone/MCM-41 mixed matrix membranes. J Memb Sci 601:117912. https://doi.org/10.1016/j.memsci.2020.117912
15. Chung TS, Chan SS, Wang R, et al (2003) Characterization of permeability and sorption in Matrimid/C60 mixed matrix membranes. J Memb Sci 211:91–99. https://doi.org/10.1016/S0376-7388(02)00385-X
16. Torresi E, Polesel F, Bester K, et al (2017) Diffusion and sorption of organic micropollutants in biofilms with varying thicknesses. Water Res. https://doi.org/10.1016/j.watres.2017.06.027
17. Xu J, Niu J, Zhang X, et al (2015) Sorption of triclosan on electrospun fibrous membranes: Effects of pH and dissolved organic matter. Emerg Contam 1:25–32. https://doi.org/10.1016/j.emcon.2015.05.002
18. Qing W, Chen J, Shi X, et al (2017) Conversion enhancement for acetalization using a catalytically active membrane in a pervaporation membrane reactor. Chem Eng J 313:1396–1405. https://doi.org/10.1016/j.cej.2016.11.053
19. Keraani A, Rabiller-Baudry M, Fischmeister C, et al (2017) First elaboration of an olefin metathesis catalytic membrane by grafting a Hoveyda–Grubbs precatalyst on zirconia membranes. Comptes Rendus Chim. https://doi.org/10.1016/j.crci.2017.04.003
20. Bai Y, Schaberg MS, Hamrock SJ, et al (2017) Density Measurements and Partial Molar Volume Analysis of Different Membranes for Polymer Electrolyte Membrane Fuel Cells. Electrochim Acta 242:307–314. https://doi.org/10.1016/j.electacta.2017.04.048
21. Wang H, da Costa JCD (2017) Membranes and fuel cells for fuel processing. Fuel Process Technol 161:. https://doi.org/10.1016/j.fuproc.2016.11.006
22. Omasta TJ, Wang L, Peng X, et al (2017) Importance of balancing membrane and electrode water in anion exchange membrane fuel cells. J Power Sources. https://doi.org/10.1016/j.jpowsour.2017.05.006
23. Alberti G, Casciola M, Massinelli L, Bauer B (2001) Polymeric proton conducting membranes for medium temperature fuel cells (110–160 °C). J Membr Sci 185:73
24. Macedonio F, Ali A, Drioli E (2017) Membrane Distillation and Osmotic Distillation. In: Reference Module in Chemistry, Molecular Sciences and Chemical Engineering
25. Luo A, Lior N (2017) Study of advancement to higher temperature membrane distillation. Desalination 419:88–100. https://doi.org/10.1016/j.desal.2017.05.020
26. Zhong W, Hou J, Yang H-C, Chen V (2017) Superhydrophobic membranes via facile bio-inspired mineralization for vacuum membrane distillation. J Memb Sci. https://doi.org/10.1016/j.memsci.2017.06.033
27. Sevelsted A, Stokholm J, Bisgaard H (2016) Risk of Asthma from Cesarean Delivery Depends on Membrane Rupture. J Pediatr 171:38-42.e4. https://doi.org/10.1016/j.jpeds.2015.12.066
28. Sun W, Ji W, Hu Q, et al (2016) Transformable DNA nanocarriers for plasma membrane targeted delivery of cytokine. Biomaterials 96:1–10. https://doi.org/10.1016/j.biomaterials.2016.04.011

29. Luk BT, Zhang L (2015) Cell membrane-camouflaged nanoparticles for drug delivery. J Control Release 220:600–607. https://doi.org/10.1016/j.jconrel.2015.07.019
30. Chung TS, Jiang LY, Li Y, Kulprathipanja S (2007) Mixed matrix membranes (MMMs) comprising organic polymers with dispersed inorganic fillers for gas separation. Prog Polym Sci 32:483–507. https://doi.org/10.1016/j.progpolymsci.2007.01.008
31. Khan AL, Cano-Odena A, Gutiérrez B, et al (2010) Hydrogen separation and purification using polysulfone acrylate-zeolite mixed matrix membranes. J Memb Sci 350:340–346. https://doi.org/10.1016/j.memsci.2010.01.009
32. Costa JAS, Garcia ACFS, Santos DO, et al (2015) Applications of inorganic-organic mesoporous materials constructed by self-assembly processes for removal of benzo[k]fluoranthene and benzo[b]fluoranthene. J Sol-Gel Sci Technol 75:495–507. https://doi.org/10.1007/s10971-015-3720-6
33. Santos DO, Santos MLN, Costa JAS, et al (2013) Investigating the potential of functionalized MCM-41 on adsorption of Remazol Red dye. Environ Sci Pollut Res 20:5028–5035. https://doi.org/10.1007/s11356-012-1346-6
34. Costa JAS, Vedovello P, Paranhos CM (2020) Use of Ionic Liquid as Template for Hydrothermal Synthesis of the MCM-41 Mesoporous Material. Silicon 12:289–294. https://doi.org/10.1007/s12633-019-00121-9
35. Santos LFS, de Jesus RA, Costa JAS, et al (2019) Evaluation of MCM-41 and MCM-48 mesoporous materials as sorbents in matrix solid phase dispersion method for the determination of pesticides in soursop fruit (Annona muricata). Inorg Chem Commun 101:45–51. https://doi.org/10.1016/j.inoche.2019.01.013
36. Costa JAS, Garcia ACFS, Santos DO, et al (2014) A new functionalized MCM-41 mesoporous material for use in environmental applications. J Braz Chem Soc 25:197–207. https://doi.org/10.5935/0103-5053.20130284
37. Costa JAS, de Jesus RA, Dorst DD, et al (2017) Photoluminescent properties of the europium and terbium complexes covalently bonded to functionalized mesoporous material PABA-MCM-41. J Lumin 192:1149–1156. https://doi.org/10.1016/j.jlumin.2017.08.046
38. Costa JAS, de Jesus RA, da Silva CMP, Romão LPC (2017) Efficient adsorption of a mixture of polycyclic aromatic hydrocarbons (PAHs) by Si–MCM–41 mesoporous molecular sieve. Powder Technol 308:434–441. https://doi.org/10.1016/j.powtec.2016.12.035
39. IARC (2010) IARC Monographs on the Evaluation of Carcinogenic Risks to Humans: Some Non-heterocyclic Polycyclic Aromatic Hydrocarbons and Some Related Exposures. Iarc Monogr Eval Carcinog Risks To Humans 92:1–868
40. U.S. EPA (1993) Provisional Guidance forQuantitative Risk Assessment of Polycyclic Aromatic Hydrocarbons. EPA/600/R-:1–28
41. Costa JAS, Sarmento VHV, Romão LPC, Paranhos CM (2019) Synthesis of functionalized mesoporous material from rice husk ash and its application in the removal of the polycyclic aromatic

hydrocarbons. Environ Sci Pollut Res 26:25476–25490. https://doi.org/10.1007/s11356-019-05852-1

42. Costa JAS, Paranhos CM (2018) Systematic evaluation of amorphous silica production from rice husk ashes. J Clean Prod 192:688–697. https://doi.org/10.1016/j.jclepro.2018.05.028
43. Costa JAS, Sarmento VHV, Romão LPC, Paranhos CM (2019) Synthesis of functionalized mesoporous material from rice husk ash and its application in the removal of the polycyclic aromatic hydrocarbons. Environ Sci Pollut Res 26:25476–25490. https://doi.org/10.1007/s11356-019-05852-1
44. Khan AL, Klaysom C, Gahlaut A, Vankelecom IFJ (2013) Polysulfone acrylate membranes containing functionalized mesoporous MCM-41 for CO2 separation. J Memb Sci 436:145–153. https://doi.org/10.1016/j.memsci.2013.02.023
45. ASTM (1995) Standard Test Methods for Water Vapor Transmission of Materials. 96–94:1–10. https://doi.org/10.1520/G0154-12A
46. Costa JAS, de Jesus RA, da Silva CMP, Romão LPC (2017) Efficient adsorption of a mixture of polycyclic aromatic hydrocarbons (PAHs) by Si–MCM–41 mesoporous molecular sieve. Powder Technol 308:434–441. https://doi.org/10.1016/j.powtec.2016.12.035
47. Costa JAS, Paranhos CM (2019) Evaluation of rice husk ash in adsorption of Remazol Red dye from aqueous media. SN Appl Sci 1:397. https://doi.org/10.1007/s42452-019-0436-1
48. Rabiller-Baudry M, Bouzin A, Hallery C, et al (2015) Evidencing the chemical degradation of a hydrophilised PES ultrafiltration membrane despite protein fouling. Sep Purif Technol 147:62–81. https://doi.org/10.1016/j.seppur.2015.03.056
49. Dorosti F, Omidkhah MR, Pedram MZ, Moghadam F (2011) Fabrication and characterization of polysulfone/polyimide-zeolite mixed matrix membrane for gas separation. Chem Eng J 171:1469–1476. https://doi.org/10.1016/j.cej.2011.05.081
50. Pavia DL, Lampman GM, Kriz GS (2001) Introduction to Spectroscopy, 3ª. Thomson Learning, Inc. 680 p., Washington D. C.
51. Helin H, Na L, Linlin W, et al (2008) Anti-fouling ultrafiltration membrane prepared from polysulfone-graft-methyl acrylate copolymers by UV-induced grafting method. J Environ Sci 20:565–570. https://doi.org/10.1016/S1001-0742(08)62095-1
52. STRUŻYŃSKA-PIRON I, BILAD MR, LOCCUFIER J, et al (2014) Influence of UV curing on morphology and performance of polysulfone membranes containing acrylates. J Memb Sci 462:17–27. https://doi.org/10.1016/j.memsci.2014.03.013

# Figures

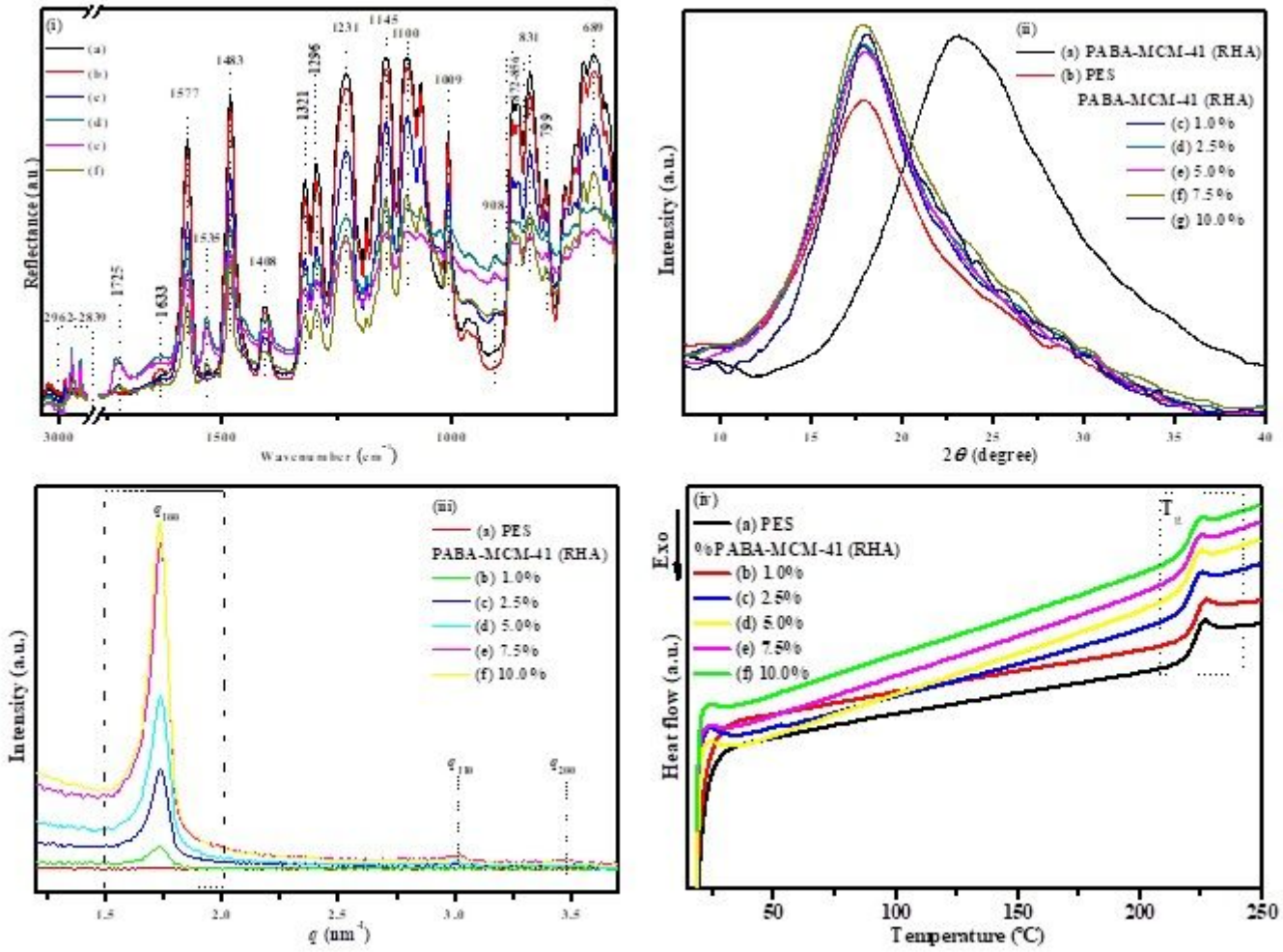


## Figure 1

ATR-FTIR spectra of PES MMMs (i), XRD profiles of PABA-MCM-41 (RHA) and PES MMMs (ii), SAXS profiles of PES MMMs (iii), and DSC curves of the second heating of PES MMMs (iv).

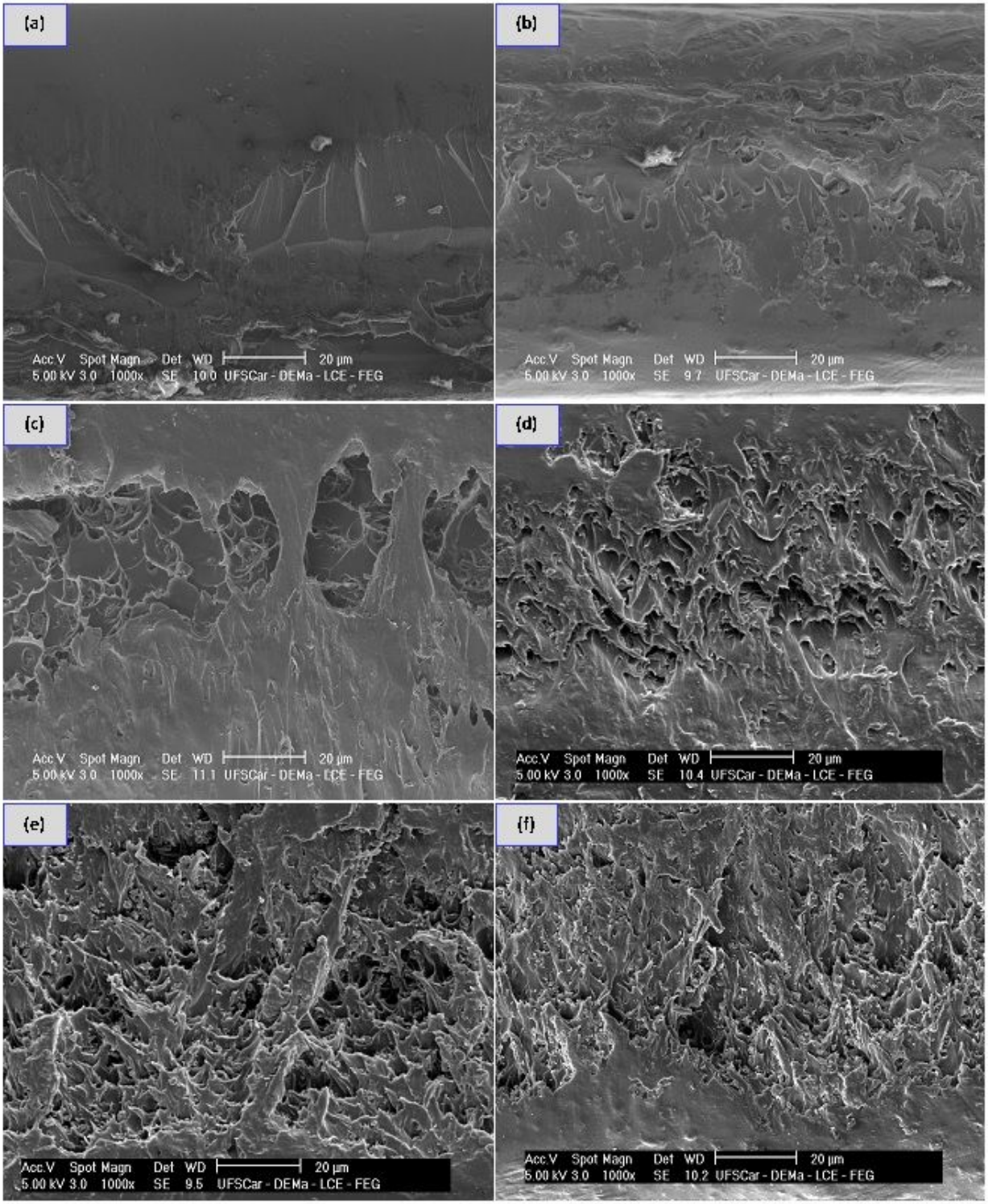


## Figure 2

Scanning electron micrograph of pristine PES membrane (a) and PES MMMs with 1.0 (b), 2.5 (c), 5.0 (d), 7.5 (e), and 10.0 wt.% (f) of PABA-MCM-41 (RHA).

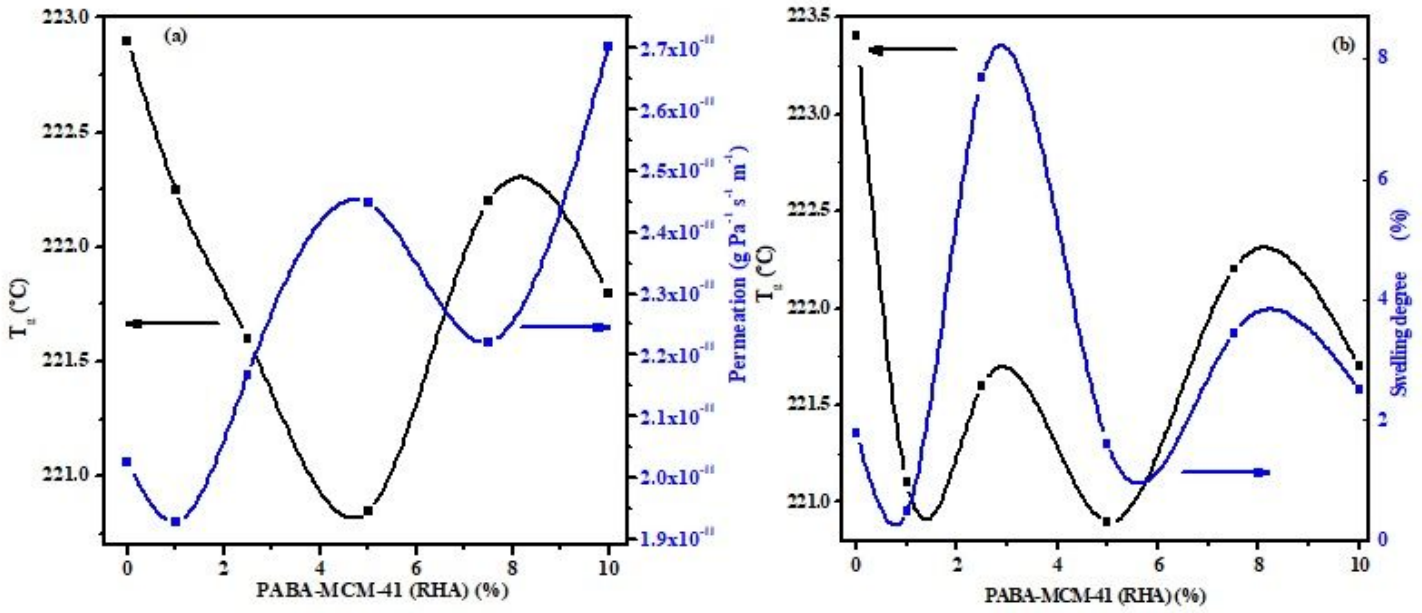


## Figure 3

Correlation between the P and Tg values (a) and water static sorption and Tg measurements (b) obtained for PES MMMs.

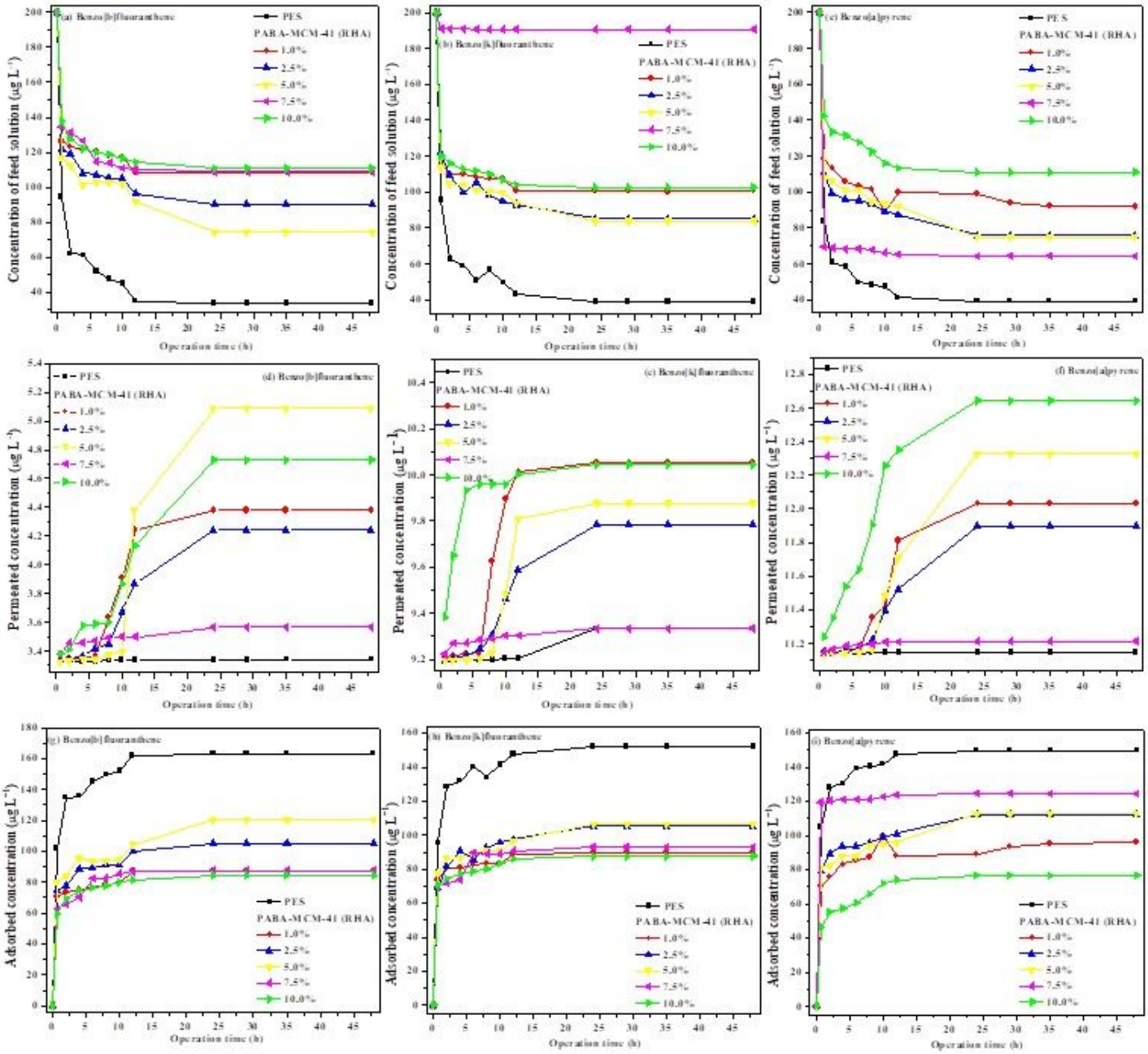


## Figure 4

Variation in PAHs concentration in feed solution (a-c), permeated concentration of PAHs solution (d-f), and adsorbed concentration of PAHs (g-i) for PES MMMs.

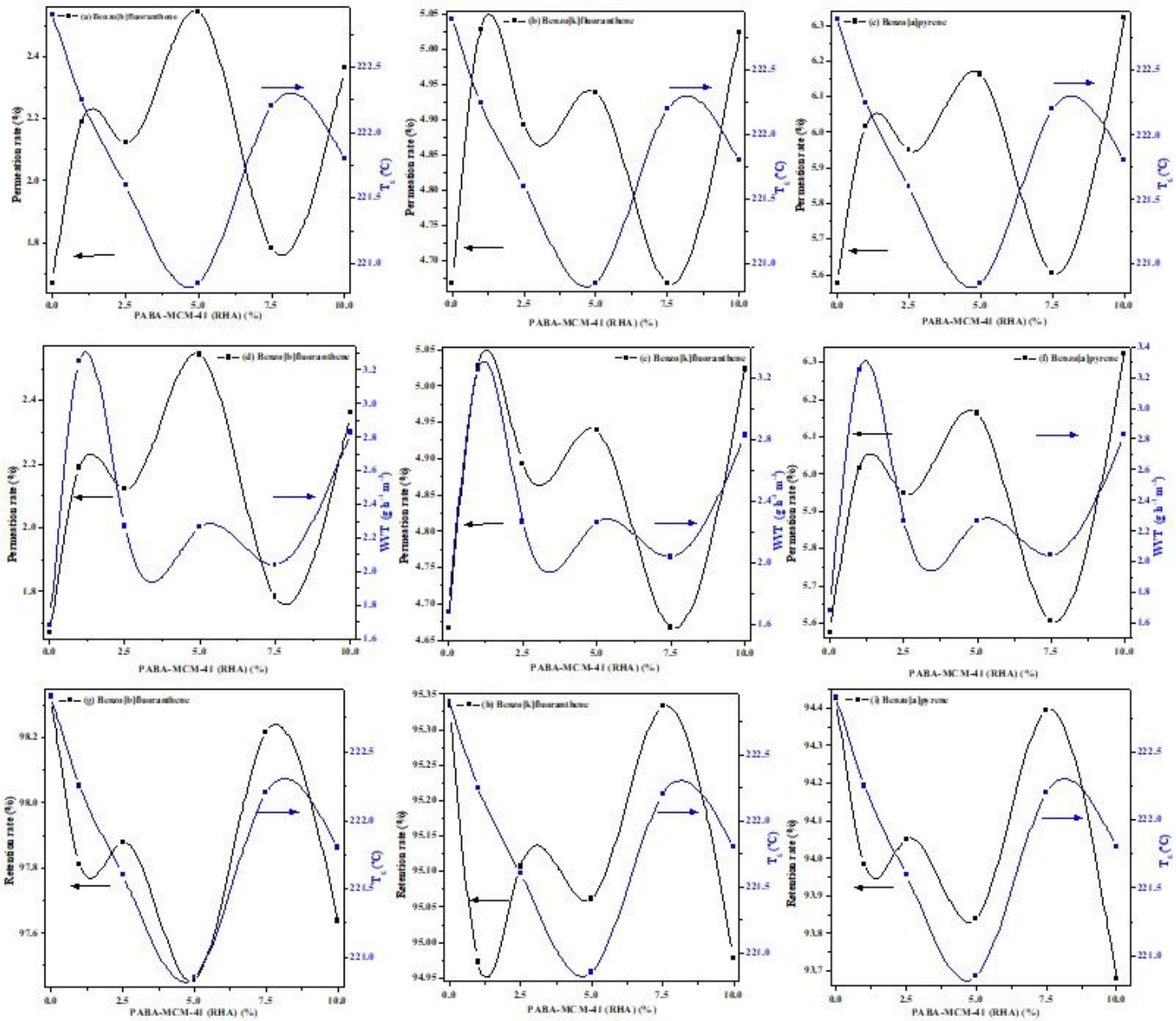


## Figure 5

Correlation between the PR and Tg (a-c), PR and WVT (d-f), and RR and Tg (g-i) values obtained for PES MMMs.

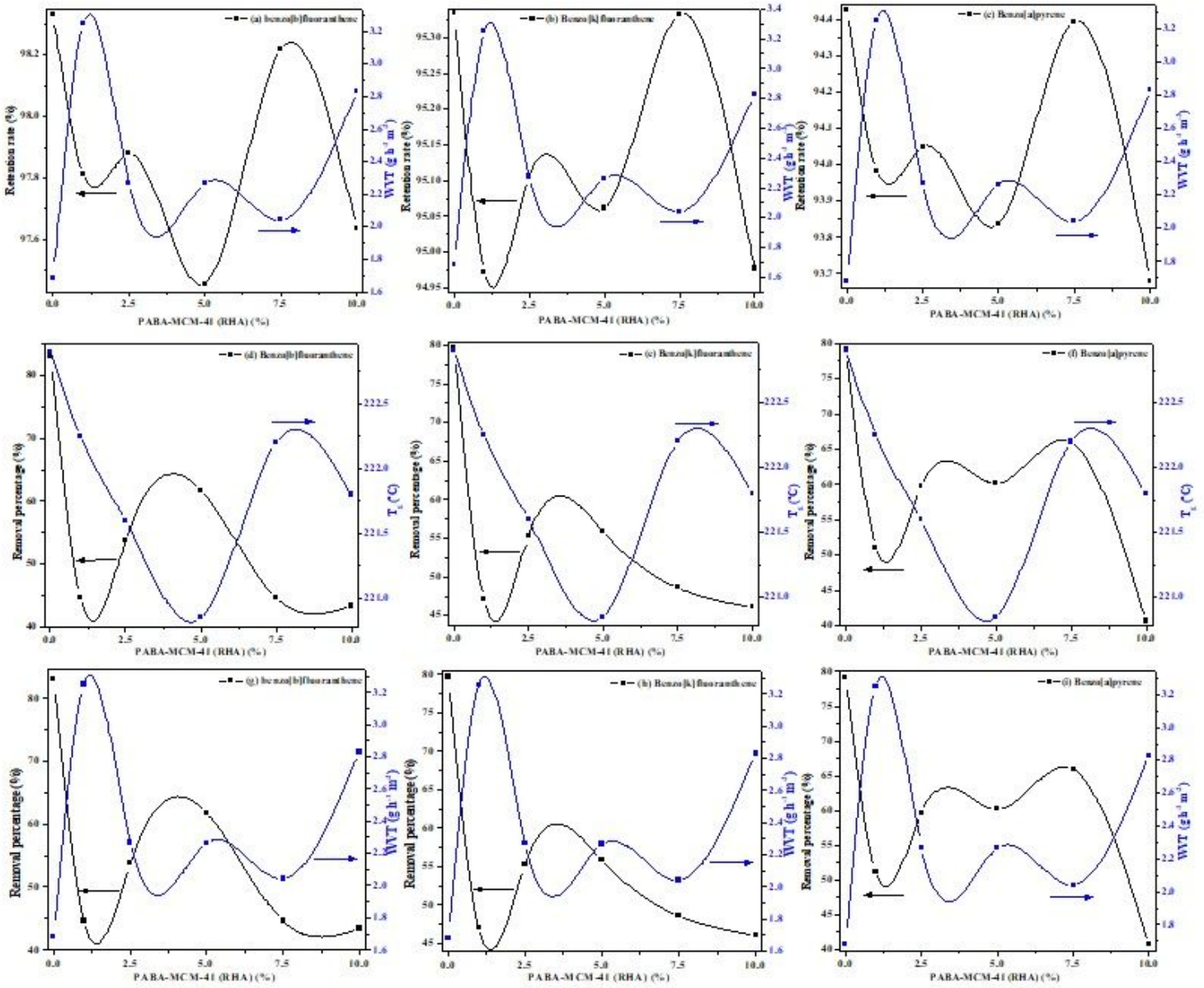


**Figure 6**

Correlation between the RR and WVT (a-c), removal percentage and Tg (d-f), and removal percentage and WVT (g-i) values obtained for PES MMMs.

# Supplementary Files

This is a list of supplementary files associated with this preprint. Click to download.

- Graphicalabstractfinal16032021.docx